

Two-stage parallel-plate energy analyzer for simultaneous detection of positive, negative, and neutral particles

D. Calabrese, O. Yenen, L. M. Wiese, and D. H. Jaecks

Behlen Laboratory of Physics, University of Nebraska, Lincoln, Nebraska 68588-0111

(Received 16 April 1992; accepted for publication 28 September 1993)

We describe a unique apparatus that simultaneously measures the laboratory energy and angles of several charged particles formed in a single beam. The ability to separate and detect particles of opposite polarity allows one to measure them in coincidence. Equations for the trajectories of the particles are derived and discussed in detail. The expressions for the corresponding resolution of the detected particles are also presented. Data produced in recent experiments illustrate some of the analyzer's more important features.

I. INTRODUCTION

For many years experimentalists have employed the parallel-plate electrostatic energy analyzer in ionic and electronic beam analysis. The most popular versions have the charged particle entering the uniform field at either 45° or 30° with respect to the plates. The first descriptions are credited to Yarnold and Bolton, Harrower, and Green and Proca.¹⁻³ Their analyses exemplify three attractive features: simplicity of construction, ease of analysis, and optimal focusing. With the introduction of position sensitive detectors (PSD),⁴⁻⁶ the parallel-plate analyzer has evolved into an instrument capable of simultaneously collecting energy and angle resolved data. A notable example is the 45° analyzer design of Roncin, Laurent, and Barat.⁷

Until recently, all parallel-plate energy analyzers separated particles of the same polarity. In some cases the concurrent measurement of the energy and angular distributions of several charged particles of different sign is important.⁸ This led Kövèr to construct a cylindrical mirror analyzer to simultaneously measure positrons and electrons.⁹

We have constructed a simple yet versatile analyzer capable of simultaneously separating positive, negative, and neutral particles from the same beam. Moreover, it allows several particles to be measured in coincidence from the same collision. The initial description of the system is discussed in Ref. 10. The analyzer consists of three parallel plates at 45° with respect to the incident beam. This is shown in Fig. 1. The midplate is at high positive potential; the front and back plates, at ground potential. Particles entering the analyzer can be measured with high resolution over a variety of laboratory angles and energies.

II. OVERVIEW OF APPARATUS

A. Description of the analyzer

The entire analyzer is shielded from magnetic fields by Conetics μ metal. Five vacuum sealed screw mechanisms outside the chamber are used for alignment when the system is under vacuum. Provisions have been made so that the analyzer may be removed and reinstalled without disturbing its alignment with respect to the initial ion beam.

The defining entrance slit on the front plate has a width (the dimension perpendicular to the plane of Fig. 1) of 263.52 mm.¹¹ The slit opening, defined by the vertical distance A in Fig. 1 (in the plane of Fig. 1 and perpendicular to the beam axis), is adjustable and currently set at 1.4200 ± 0.0025 mm. As measured from the center of our collision cell, the width is large enough to accept particles scattered as much as 5° in the laboratory frame. The scattering plane is defined by the triangle formed by the collision center and the line bisecting the slit opening horizontally. In Fig. 2 this is shown as the plane RPV.

The front plate of the analyzer has dimensions 812.80 mm \times 520.70 mm \times 12.7 mm on which one can place several detectors. Because the area is large, several detectors can be used to simultaneously measure several particle energies and scattering angles, relative to the collision center. The large area also allows for easy repositioning of the detectors.

The midplate has dimensions 635 mm \times 460.38 mm \times 4.85 mm. The mid plate, which is 177.74 mm behind the analyzer front plate, consists mostly of a 96% transmission wire mesh (see dashed line in Fig. 1). The mesh is hand wound in only one direction, parallel to the projection of the initial beam direction onto the plate, with 0.12-mm-diam wire. The wires are spaced 6.34 mm apart. The mesh helps keep the field uniform while allowing particles to pass through the middle plate and reach their respective detectors. In addition, its small size minimizes the possibility of particles hitting it and scattering into the detectors on the front plate.

For a primary H_3^+ beam and a suitable positive voltage on the midplate, protons are deflected away from the beam toward the front plate; particles such as H and H_2 (shown as neutrals N_0 in Fig. 1), H_2^+ , H_3^+ , and H^- reach their detectors behind the back plate. Therefore, it is possible to measure the energy distributions of several dissociation fragments of various charges and masses at one time.

In between each stage of the analyzer, 1.58-mm-thick guard plates have been placed to help keep the fields uniform (see Fig. 1). Each plate, including the front, back, and midplates, is electrically connected to the preceding plate by a 3.0 M Ω precision resistor, forming a voltage divider network between the midplate and the front plate, and between the midplate and the back plate. The resistors

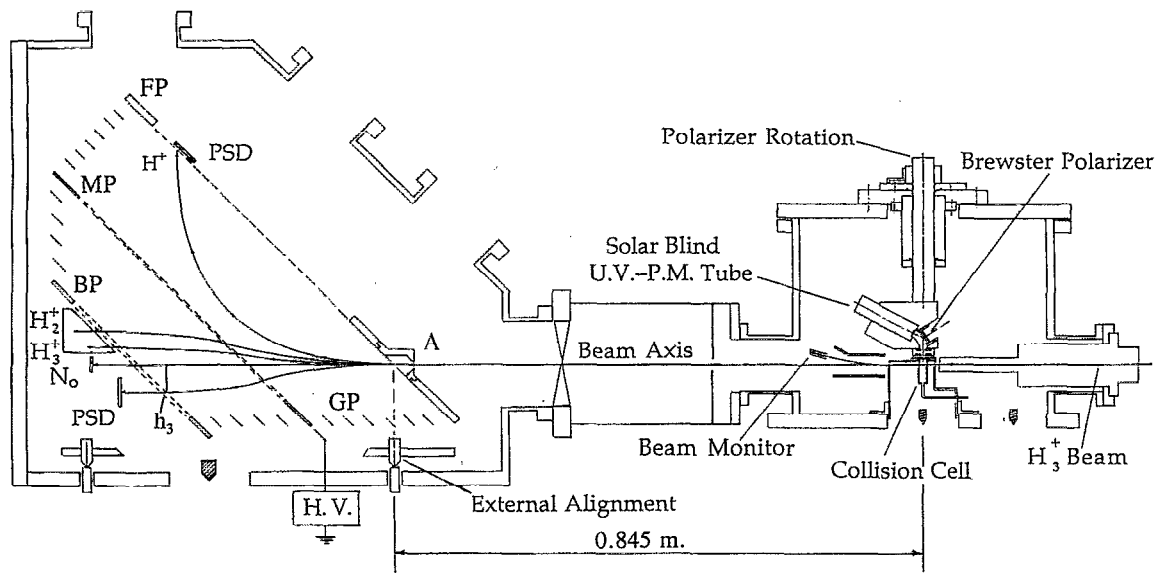


FIG. 1. Cross-sectional view of analyzer showing the trajectories of various particles to their corresponding detectors. The abbreviations FP, MP, BP, and GP represent the front plate, midplate, backplate, and guard plates, respectively. The dashed line shown on the midplate represents the hand wound mesh discussed in Sec. II. The symbol A represents the slit opening. h_3 is the perpendicular distance from the point where the negatively charged particles intersect the back plate, to the scattering plane. Also shown is the rest of the experimental apparatus, including the collision chamber.

are inside the vacuum chamber and have matched temperature coefficients of 15 ppm/°C (parts per million per °C). The center-to-center spacing between plates in the front stage is 25.40 mm whereas in the back stage it is 26.34 mm.

The first guard plate (behind the front plate), has inner and outer dimensions 711.20 mm × 384.18 mm and 787.40 mm × 460.38 mm, respectively. Furthermore, the height of each successive plate decreases gradually to make the an-

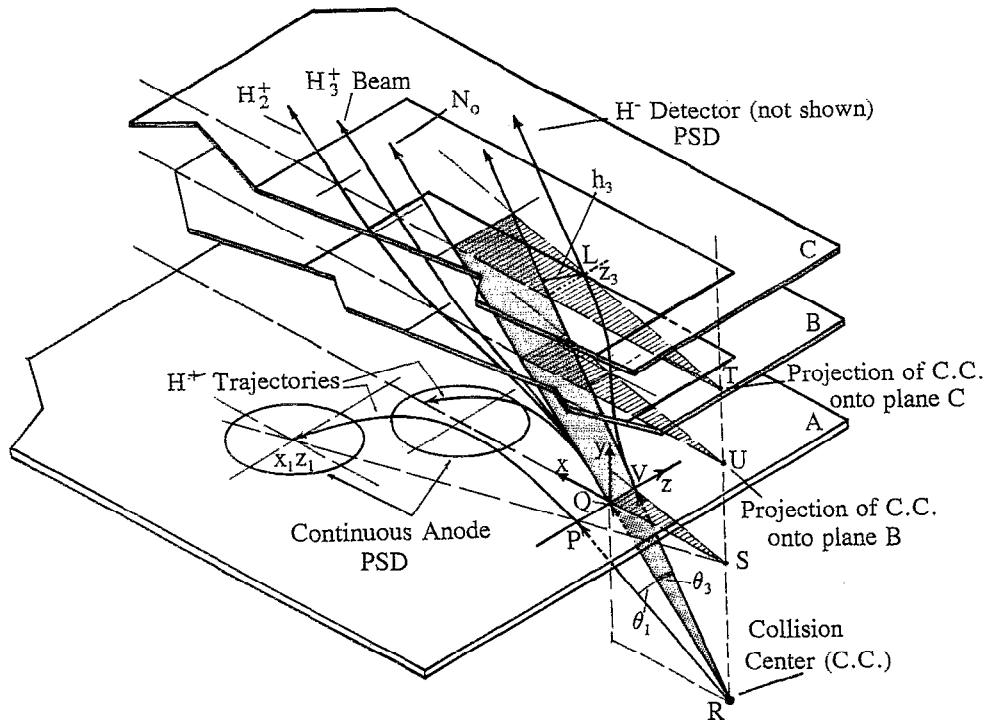


FIG. 2. The front (plane A), the mid (plane B), and the back (plane C) plates of the analyzer along with representative trajectories of various particles. R denotes the collision center and S, U, and T represent the projection of the collision center onto the planes A, B, and C, respectively. The shaded plane (plane RQV) is the scattering plane. The hatched planes are the projection of the scattering plane onto the plates (planes A, B, and C). Q is the geometrical center of the slit and the origin of the xyz coordinate system shown. The line PV is along the slit and bisects it. θ_1 is the scattering angle of the proton which lands on a position sensitive detector (PSD) on the front plate. x_1 and z_1 are the coordinates of the proton as determined by the PSD. θ_3 is the scattering angle of the H^- . L is the point where the trajectory of the H^- intersects the plane C (back plate). At the back plate, the displacement of the trajectory of H^- is specified by the coordinate z_3 and the length h_3 which is the perpendicular distance of L from the scattering plane RQV.

alyzer fit in the vacuum chamber at 45° (see Fig. 1).

In the following analysis we will derive our equations for an idealized case and neglect the effects of meshes and guard plates. In reality, the effects of meshes and guard plates cannot be neglected *a priori*, especially when considering analyzers with ideal resolution of 1% or better.

B. Design criteria

It is well known that the optimum conditions for first order focus and resolution are the same: particles must enter the analyzer at 45° with respect to the plates.^{1,2} Figure 2 shows the front (plate A), the mid (plane B), and back (plane C) plates along with representative trajectories for H⁺, H₂⁺, H₃⁺, H⁻, and neutrals (H or H₂, represented by N₀). R denotes the collision center and S is its projection onto plane A (front plate's plane). The projections of the collision center onto the plane B and C are shown by U and T, respectively. Note that these intersections are out of the plates, since the plates do not extend to the line passing through the collision center and S. Each trajectory with its corresponding laboratory scattering angle defines a plane that is perpendicular to the analyzer's plates. For example, particles scattered at 0° and at θ₃ are confined to the planes RQS and RVS, respectively. We define a right-handed rectangular coordinate system with its x axis in the front plate's plane (plane A), parallel to the projection of the beam direction onto plane A, as shown in Fig. 2. The y axis of this coordinate system is perpendicular to plane A, directed from plane A to plane B. The z axis is also in plane A and perpendicular to both x and y axes. Thus, the acceleration in the analyzer is confined to the y direction. The origin of the coordinate system is at the geometrical center of the entrance slit (point Q in Fig. 2).

For the various charged particles entering the analyzer, the initial velocity components along the directions x, y, and z are

$$v_{0x} = v_0 \cos \theta \cos \alpha, \quad (1a)$$

$$v_{0y} = v_0 \cos \theta \sin \alpha = v_0 \sin \gamma, \quad (1b)$$

$$v_{0z} = v_0 \sin \theta, \quad (1c)$$

where θ is the laboratory scattering angle; γ, the injection angle for a laboratory scattering angle of θ; and α = π/4, the injection angle at θ = 0°. Due to the finite entrance slit dimensions, there is an uncertainty Δα in the angle α.

For a positively charged particle landing on the front plate (plane A, Fig. 2). The range of its parabolic path is

$$R = R_0 \sin 2\gamma = 2R_0 \sin \gamma \cos \gamma, \quad (2a)$$

where

$$R_0 = \frac{2E_+ d_1}{qV_{an}}. \quad (2b)$$

Using Eq. (1b), we get

$$R = 2R_0 \sin \alpha \cos \theta_1 \sqrt{1 - \sin^2 \alpha \cos^2 \theta_1}, \quad (2c)$$

where E₊ is the laboratory energy of the positively charged particle produced in the collision cell; V_{an} the potential applied to the analyzer; q the charge; d₁ the distance between the midplate and the front plate; and θ₁ the laboratory scattering angle. Our present slit opening yields a Δα of ±0.051° as measured from the center of the collision cell. In that case, using Eq. (2a), the departure from first-order focusing (θ₁ = 0 and α = 45°) is 1.586 × 10⁻⁶ R₀ (see also Yarnold *et al.*¹). Combining Eqs. (2b) and (2c), we get

$$E_+ = \frac{RqV_{an}}{4d_1 \sin \alpha \cos \theta_1 \sqrt{1 - \sin^2 \alpha \cos^2 \theta_1}}. \quad (2d)$$

The analyzer resolution can be computed by applying standard error analysis techniques to Eq. (2d). For α = 45°, the full width at half-maximum (FWHM) resolution is

$$\left(\frac{\Delta E_+}{E_+}\right)_{\text{FWHM}} = \frac{1}{2} \left[\left(\frac{\Delta V_{an}}{V_{an}}\right)^2 + \left(\frac{\Delta d_1}{d_1}\right)^2 + \left(\frac{\Delta R}{R}\right)^2 + \left(\tan \theta_1 - \frac{\sin(2\theta_1)}{2(2 - \cos^2 \theta_1)}\right)^2 (\Delta \theta_1)^2 + \left(\frac{2 \sin^2 \theta_1}{\cos^2 \theta_1 - 2}\right)^2 (\Delta \alpha)^2 \right]^{1/2}, \quad (3)$$

where ΔR is the sum of the entrance slit opening and the image resolution of the positive particle detector. For our present detector configuration, the ideal FWHM resolution is 0.33% according to Eq. (3). The main contribution of the resolution comes from the ΔR/R term. The contributions to the resolution from the angular terms are estimated to be about 0.001% for θ₁ as large as 5°.

Equations (2a)–(2d) are the more familiar forms for the parabolic motion of the charged particles. However in real situations the values of E₊ and θ₁ have to be determined from the measured quantities. To do so, it is more convenient to use the Cartesian components x₁ and z₁ of the range for the coordinate system we have already described. From the geometry, we find for any α

$$x_1 = R_0 \cos^2 \theta_1 \sin 2\alpha, \quad (4a)$$

$$z_1 = R_0 \sin 2\theta_1 \sin \alpha + \frac{L_0 \tan \theta_1}{\sqrt{2} \sin \alpha}, \quad (4b)$$

where θ₁ is the scattering angle of the particle, and where L₀ = 0.845 m is the distance from the collision center to the entrance slit. R₀ is given by Eq. (2b). Solving these equations for E₊ and θ₁ we get

$$\tan \theta_1 = \frac{z_1}{(x_1/\cos \alpha) + (L_0/\sqrt{2} \sin \alpha)}, \quad (5a)$$

$$E_+ = \frac{qV_{an}}{2d_1 \sin 2\alpha} \left(1 + \frac{z_1^2}{[(x_1/\cos \alpha) + (L_0/\sqrt{2} \sin \alpha)]^2} \right). \quad (5b)$$

From the geometry of Fig. 2 the negatively charged particles deflect away from the beam with coordinates h₃ and z₃. If the surface of the detector is parallel to and

directly behind the back plate (plane C in Fig. 2), the negative particles hit the detector at point L, shown in Fig. 2. We define h_3 as the perpendicular distance from point L to the scattering plane RQV. z_3 is the z coordinate of L, i.e., the perpendicular distance from the point L to the RSQ plane (the plane which would contain particles scattered at 0°). One can show that h_3 and z_3 can be written as (see Appendix for the case when the particle has positive charge)

$$h_3 = \frac{1}{\sqrt{2}} (d_1 + d_2) \left[2\rho_3 \cot \alpha \left(1 - \sqrt{1 + \frac{1}{\rho_3}} \right) + 1 \right] - \frac{T}{\sqrt{2}} \left[\frac{\cot \alpha}{\sqrt{1 + (1/\rho_3)}} - 1 \right] + \frac{L_0}{2} (1 - \cot \alpha), \quad (6a)$$

$$z_3 = \left[(d_1 + d_2 + T) + \frac{L_0}{\sqrt{2}} - \sqrt{2}h_3 \right] \frac{\tan \theta_3}{\cos \alpha}, \quad (6b)$$

where

$$\rho_3 = \frac{kE_- \sin^2 \alpha \cos^2 \theta_3}{E_+} = \frac{E_- \sin^2 \alpha \cos^2 \theta_3}{|qV_{an}|}. \quad (6c)$$

E_- is the laboratory energy of the negatively charged particle produced in the collision cell; d_2 the distance between the midplate and the back plate; T the thickness of the

midplate; L_0 the distance from the collision center to the analyzer entrance slit; θ_3 the laboratory scattering angle; and $k = R_0/2d_1$ the analyzer constant. In real situations, the values of E_- and θ_3 have to be determined from the measured quantities (h_3 and z_3), the geometrical dimensions (d_1 , d_2 , T , L_0 , α), and the voltage V_{an} on the midplate using the Eqs. (6a), (6b), and (6c). The dependence on V_{an} is in E_+ through Eq. (2d).

Since Eq. (6a) is cumbersome, we have approximated it by neglecting $\Delta\alpha$, inverting and then numerically fitting $kE_- \cos^2 \theta_3/E_+$ to terms containing $1/h_3$, h_3 , and a constant. A plot of $kE_- \cos^2 \theta_3/E_+$ versus h_3 shows that this function behaves hyperbolically for small h_3 , while for larger h_3 it behaves linearly. Therefore, Eq. (6a) is approximated as

$$\frac{kE_- \cos^2 \theta_3}{E_+} \approx a + ch_3 + \frac{b}{h_3}, \quad (7)$$

where $a = -1.0152$, $b = 0.112944$ m, and $c = 2.2806/\text{m}$. The approximation is within 0.005% of the theoretical value for all h_3 between 0.51 and 101.60 mm. For our typical measurements, h_3 will usually be about 50 mm. Using the very good approximation of Eq. (7), we find the resolution for E_- to be

$$\left(\frac{\Delta E_-}{E_-} \right)_{\text{FWHM}} \approx \sqrt{\tan^2 \theta_3 (\Delta \theta_3)^2 + \frac{(-b + ch_3^2)^2 (\Delta h_3)^2}{4(ah_3^2 + bh_3 + ch_3^3)^2} + \left(\frac{\Delta E_+}{E_+} \right)_{\text{FWHM}}^2}, \quad (8)$$

where Δh_3 is the sum of the slit opening distance and image resolution of the negatively charged particle detector. The values of θ_3 and $\Delta \theta_3$ are obtained from the measured quantities (z_3 and h_3) and the geometrical dimensions (d_1 , d_2 , T , and L_0) in Eq. (6b). For our system, the main contribution to the energy resolution of the negatively charged particle comes from the second term under the radical. As an example, let us consider a position sensitive detector utilizing microchannel plates. For this type of detector an image resolution of approximately 100 μm is possible.⁵ Therefore, the ideal resolution for $\theta_3 = 0^\circ$ and $h_3 = 50$ mm is about 2.6% according to Eq. (8). The reason for this low resolution number is that the energy dependence of the deflection of the negatively charged particle below the beam axis is not strong enough for good energy analysis. Therefore, to improve the resolution, time-of-flight differences between the positively and the negatively charged particles should be used. In this method, the arrival time difference between the positive and the negative particles is accurately measured. The time-of-flight of the positive particle is accurately determined since its velocity can be obtained from its accurately measured energy and the distance it has traveled is known from geometrical considerations. From these, the time-of-flight of the negatively charged particle is obtained. Knowing the distance

traveled by the negative particle, its velocity, and hence its energy, is determined. For example, in $\text{H}^+ - \text{H}^-$ coincidences obtained at 0° from the dissociation of $(\text{H}_2)^*$ formed in 4.0 keV $\text{H}_2^+ - \text{He}$ collisions, the arrival time difference between H^+ and H^- is about 500 ns. Using standard error analysis techniques applied to the time-of-flight equations and assuming that: (1) the time resolution of the electronics is 1.0 ns, (2) the uncertainty in the measurements of the distance traversed by each particle is 0.80 mm, (3) the slit opening of the analyzer is 1.42 mm, and (4) image resolution of the detectors is 100 μm , the previously quoted ideal resolution of 2.6% can be improved to 0.42%. In this case, the main source of uncertainty is the energy resolution of the proton [see Eq. (3)].

Particles of positive charge which are too energetic to be collected on the front plate, are detected behind the back plate. They are deflected above the beam with coordinates h_2 and z_2 . One can show that h_2 and z_2 are (a detailed derivation is given in the Appendix)

$$h_2 = \frac{1}{\sqrt{2}} (d_1 + d_2) \left[2\rho_2 \cot \alpha \left(1 - \sqrt{1 - \frac{1}{\rho_2}} \right) - 1 \right] + \frac{T}{\sqrt{2}} \left(\frac{\cot \alpha}{\sqrt{1 - (1/\rho_2)}} - 1 \right) - \frac{L_0}{2} (1 - \cot \alpha), \quad (9a)$$

$$z_2 = \left[(d_1 + d_2 + T) + \frac{L_0}{\sqrt{2}} + \sqrt{2}h_2 \right] \frac{\tan \theta_2}{\cos \alpha}, \quad (9b)$$

where

$$\rho_2 = \frac{kE \cos^2 \theta_2 \sin^2 \alpha}{E_+} = \frac{E \cos^2 \theta_2 \sin^2 \alpha}{|qV_{an}|}. \quad (9c)$$

θ_2 is the laboratory scattering angle and E is the laboratory energy of the positively charged particle produced in the

collision cell. Again, because of the complexity of Eq. (10) we fit $kE \cos^2 \theta/E_+$ to the coordinate h_2 . The fit yields

$$\frac{kE \cos^2 \theta_2}{E_+} = n + ph_2 + \frac{q}{h_2}, \quad (10)$$

where $n=1.0156$, $p=2.2685/m$, and $q=0.112944 m$. The approximation is within 0.005% of the actual value for $0.51 \text{ mm} < h_2 < 115.82 \text{ mm}$. Thus, to a very good approximation the energy resolution is

$$\left(\frac{\Delta E}{E} \right)_{\text{FWHM}} \approx \sqrt{\tan^2 \theta_2 (\Delta \theta_2)^2 + \frac{(-q + ph_2^2)^2 (\Delta h_2^2)}{4(nh_2^2 + qh_2 + ph_2^3)^2} + \left(\frac{\Delta E_+}{E_+} \right)_{\text{FWHM}}^2}. \quad (11)$$

Since it is possible to install two or more detectors for particles deflected above the beam, one can perform coincidence measurements between several particles of positive charge as well as particles of opposite polarity (see Fig. 1).

III. EXAMPLES

Laboratory energy spectra of protons produced at 0° from 4.0 keV H_3^+ and H_2^+ collisions with He have been measured with this analyzer.^{12,14} Similar distributions for H^- from 2.417 to 7.0 keV collisions with He have also been measured.¹³

A major test of our system for future coincidence experiments has been to determine whether any $\text{H}^+ - \text{H}^-$ coincidences could be observed for the collision induced dissociation of H_3^+ by He targets. We have obtained data for these coincidences at 4.0 keV for protons at 0° and 0.17° in the laboratory frame.¹⁵ Acceptance angles for the protons and H^- are $\pm 0.024^\circ$ and $\pm 0.25^\circ$, respectively. Because of the limited range of the H^- detector used in this experiment, not all possible coincidences are seen. Figure 3(a) shows a typical sample of time spectra obtained from the start-stop coincidence method.¹⁶ Such a spectrum shows the distribution of the elapsed time between a pulse pro-

duced by the H^- detector and another pulse produced by the H^+ detector. Time correlated events (true coincidences) manifest themselves as a peak on top of a background in the coincidence time spectrum. The background is due to uncorrelated coincidence events (accidental coincidences). The area under the peak above the background gives the total number of time correlated events. Figure 4 shows the number of coincidences between H^+ and H^- produced along the beam axis as a function of the analyzer voltage. For comparison, the laboratory energy distribution of protons from the dissociation of H_3^+ is also shown. Data accumulation times vary from 10 to 144 h. It is obvious from Fig. 4 that few protons are produced in coincidence with the H^- at 896 V. Complete details of this experiment are presented in another article.¹⁵

The analyzer's versatility allows one to make a host of measurements. One can study the dissociation mechanisms of two, three, and four-body systems. An example is H_3^+ . One possibility is to measure the three-body breakup of H_3^+ into $\text{H}^+ + \text{H}^- + \text{H}^+$ in a triple coincidence experiment. Thus, one can study several fundamental issues such as

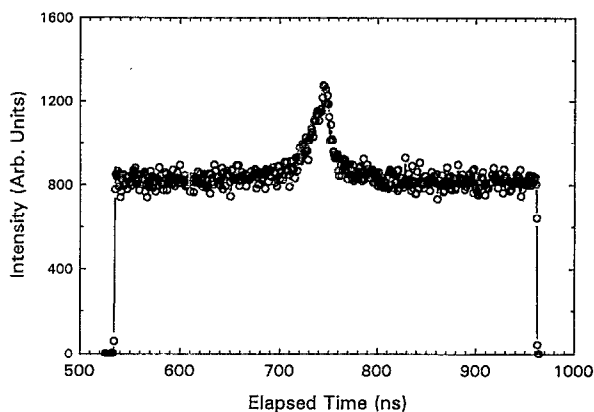


FIG. 3. (a) Time spectrum of $\text{H}^+ - \text{H}^-$ coincidences obtained at 0° from 4.0 keV H_3^+ collisions with He. The voltage of the midplate is set to 906 V.

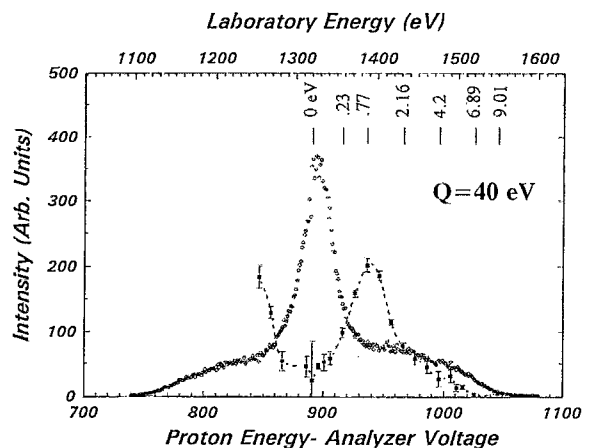


FIG. 4. Total number of real coincidences (filled squares) as a function of analyzer voltage with the laboratory energy distribution of protons (open circles). The latter data are from Ref. 15. The top scale corresponds to the laboratory energies of the protons. The vertical lines represent center of mass energies of the protons.

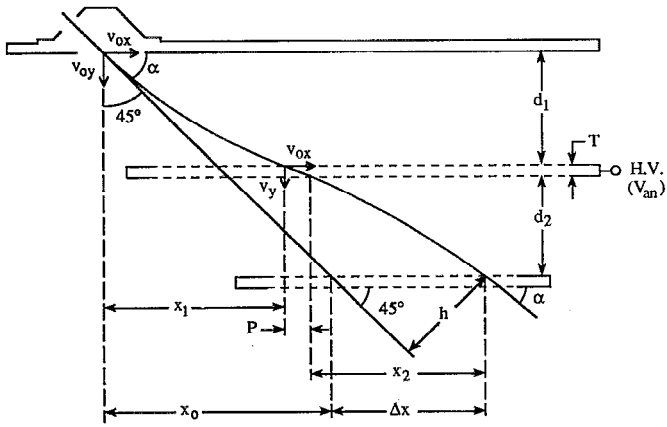


FIG. 5. A schematic view of the x - y plane (RSQ plane in Fig. 2). The figure is not drawn to scale to emphasize details needed in the Appendix. The straight line at 45° is the beam direction. Neutrals arriving at $\theta=0^\circ$ and $\alpha=45^\circ$ follow this path. The continuous curve is the projection of the trajectory of a particle with arbitrary θ and α , onto the x - y plane.

how the energy is shared between the two H^+ ions, and what is the distribution of the angle between these two protons in the center of mass of the dissociating H_3^+ . This three-body dissociation study would produce valuable information on the behavior of three Coulomb-interacting particles.

APPENDIX

This appendix gives a detailed derivation of Eqs. (9a) and (9b). Equations (6a) and (6b) can be derived in a similar way. In this case we focus on positively charged particles when the positive voltage on the midplate is not high enough to bend the trajectory completely towards the front plate. We use the right handed coordinate system defined in Sec. II B and shown in Fig. 2.

Figure 5 shows the x - y plane for this coordinate system (RSQ plane in Fig. 2). The straight line in the figure is the beam direction ($\theta=0^\circ$, $\alpha=45^\circ$). Neutral particles arriving at the center of the slit would follow this trajectory. The continuous curve is the projection onto the x - y plane of the trajectory of a positively charged particle. We specify the arbitrary direction of this particle by two angles: θ is the angle between the velocity vector and the x - y plane; α is the angle between the x axis and the projection of the velocity vector onto the x - y plane.

The acceleration a_1 is the acceleration of the charged particle due to the electric field between the mid and front plates, which are separated by the distance d_1 . Similarly, a_2 is the acceleration of the particle due to the electric field between the mid and back plates, which are separated by the distance d_2 . If the analyzer voltage is V_{AN} , then

$$a_1 d_1 = a_2 d_2 = \frac{qV_{AN}}{m}. \quad (12)$$

Let t_1 be the time it takes a charged particle of mass m to travel from the entrance slit to the midplate. From the equations of motion

$$v_y = v_{0y} - a_1 t_1 = \sqrt{v_{0y}^2 - 2a_1 d_1}, \quad (13)$$

where v_y is the y component of the velocity at the midplate. The y component of the initial velocity, v_{0y} can be written as

$$v_{0y} = \sqrt{\frac{2E}{m}} \cos \theta \sin \alpha. \quad (14)$$

Substituting Eqs. (12) and (14) into Eq. (13) and solving for t_1 , we get

$$t_1 = \frac{m d_1}{q V_{AN}} \sqrt{\frac{2E}{m}} \cos \theta \sin \alpha \left[1 - \sqrt{1 - \frac{q V_{AN}}{E \cos^2 \theta \sin^2 \alpha}} \right]. \quad (15)$$

To calculate the time t_2 it takes for a particle to traverse the region between the mid and back plates it is more convenient to consider the time-reversed motion since t_2 does not depend on the direction of travel, for fixed speeds and angles at the plates. The energy conservation law insures that the exit velocity vector of a particle at the back plate is the same as its velocity vector at the entrance slit. Thus, when we consider the time-reversed motion, the initial velocity of the particle at the back plate is the same as the velocity at the entrance slit except it has the opposite direction. Therefore, the expression for t_2 is similar to Eq. (15) for particles moving backwards, from the back plate to the midplate under the influence of the acceleration a_2 between the back and midplates

$$t_2 = \frac{m d_2}{q V_{AN}} \sqrt{\frac{2E}{m}} \cos \theta \sin \alpha \left[1 - \sqrt{1 - \frac{q V_{AN}}{E \cos^2 \theta \sin^2 \alpha}} \right]. \quad (16)$$

At the midplate, we assume that the region between the front and back faces of the mesh is field-free. Let P be the x component of the displacement. P is related to the thickness T of the midplane through

$$\frac{P}{T} = \frac{v_{0x}}{v_y} = \frac{v_{0x}}{\sqrt{v_{0y}^2 - 2a_1 d_1}}, \quad (17)$$

$$P = T \cot \alpha / \sqrt{1 - \frac{q V_{AN}}{E \cos^2 \theta \sin^2 \alpha}}. \quad (18)$$

From Fig. 5, $\Delta x = x_1 + P + x_2 - x_0$ where $x_1 = v_{0x} t_1$, $x_2 = v_{0x} t_2$, and $x_0 = (d_1 + d_2 + T)$. In the following analysis, the surface of the detector is parallel and directly behind the back plate. We also neglect the thickness of the back plate. In a more refined analysis, the back plate thickness has to be taken into account. In the case where the back plate thickness is neglected, let L be the point where the particle hits the detector. We define h as the perpendicular distance from the point L to the scattering plane (which is the RQV plane in Fig. 2). This distance is also marked as h in Fig. 5 since the actual trajectory is projected perpendicularly to x - y plane. From the geometry of Fig. 5 we get

$$h = \frac{1}{\sqrt{2}} \Delta x. \quad (19)$$

Substituting the expressions for v_{0x} , t_1 from Eq. (15), t_2 from Eq. (16), and P from Eq. (18), we get

$$h = \frac{1}{\sqrt{2}} (d_1 + d_2) \left[2\rho_2 \cot \alpha \left(1 - \sqrt{1 - \frac{1}{\rho_2}} \right) - 1 \right] + \frac{T}{\sqrt{2}} \left(\frac{\cot \alpha}{\sqrt{1 - (1/\rho_2)}} - 1 \right), \quad (20)$$

where, to write this equation in compact form, we have used the dimensionless variable ρ_2 given by Eq. (9c).

Equation (20) gives the value of h for the deflection of the particle while in the analyzer. However, due to finite slit opening, the particles that enter at an arbitrary injection angle will have an additional displacement acquired during their travel from the collision center to the entrance slit. The law of sines applied to the triangle formed by the collision center, center of the slit, and the projection of the point of entrance of the particle (the point where the trajectory intersects the plane of the entrance slit) onto the x - y plane, gives

$$\frac{x_b}{\sin(\Delta\alpha)} = \frac{L_0}{\sin \alpha}, \quad (21)$$

where x_b is the side of the triangle opposite to the angle $\Delta\alpha$. Since x_b makes an angle of 45° with the direction of h , the needed correction is

$$\frac{x_b}{\sqrt{2}} = \frac{L_0}{2} (\cot \alpha - 1), \quad (22)$$

which must be added to the total displacement. The result is Eq. (9a).

To calculate the total deflection in the z direction, we consider the time it takes for the particle to travel from the collision center to the analyzer's back plate. Since x and z components of the velocity do not change, this time can be expressed as

$$\frac{x_{\text{total}}}{v_{0x}} = \frac{z_2}{v_{0z}}, \quad (23)$$

where $x_{\text{total}} = (L_0/\sqrt{2}) + x_0 + \Delta x$. Substituting the values of $x_0 = (d_1 + d_2 + T)$, Δx from Eq. (19), and v_{0z}/v_{0x} ratio from Eqs. (1a) and (1c) we obtain Eq. (9b).

ACKNOWLEDGMENTS

The support of this work by the National Science Foundation under Grant No. PHY-9120213 is gratefully acknowledged. We would especially like to thank Mr. Jack Loos for his contributions to the design and construction of the apparatus.

- ¹Rev. G. D. Yarnold and H. C. Bolton, *J. Sci. Instrum.* **26**, 38 (1949).
- ²G. A. Harrower, *Rev. Sci. Instrum.* **26**, 850 (1955).
- ³T. S. Green and G. A. Proca, *Rev. Sci. Instrum.* **41**, 1409 (1970).
- ⁴R. C. G. Leckey, *J. Electron Spectrosc. Relat. Phenom.* **43**, 183 (1987).
- ⁵C. Martin, P. Jelinski, M. Lampton, R. F. Malina, and H. O. Anger, *Rev. Sci. Instrum.* **52**, 1067 (1981).
- ⁶J. L. Alberi and V. Radeka, *IEEE Trans. Nucl. Sci. NS* **23**, 251 (1976).
- ⁷P. Roncin, H. Laurent, and M. Barat, *J. Phys. E* **19**, 37 (1986).
- ⁸J. S. Briggs, *Comments At. Mol. Phys.* **23**, 155 (1989).
- ⁹A. Köver, *Meas. Sci. Technol.* **2**, 448 (1991).
- ¹⁰O. Yenen, D. H. Jaecks, and L. Xing, *Fifteenth International Conference on the Physics of Electronic and Atomic Collisions, Abstracts of Contributed Papers*, Brighton 1987 (North-Holland, Amsterdam, 1987), p. 803.
- ¹¹All dimensions are measured to ± 0.001 in. = 0.0254 mm unless otherwise stated. The main exception to this is the slit opening, measured to ± 0.0001 in. which is measured using a traveling microscope.
- ¹²O. Yenen, L. M. Wiese, D. Calabrese, and D. H. Jaecks, *Phys. Rev. A* **42**, 324 (1990).
- ¹³O. Yenen, D. H. Jaecks, and L. M. Wiese, *Phys. Rev. A* **39**, 1767 (1989).
- ¹⁴D. H. Jaecks, O. Yenen, L. Wiese, and D. Calabrese, *Phys. Rev. A* **41**, 5934 (1990).
- ¹⁵O. Yenen, D. Calabrese, L. M. Wiese, D. H. Jaecks, and G. A. Gallup, *Phys. Rev. A* **47**, 1059 (1993).
- ¹⁶C. Dupré, A. Lahmam-Bennani, and A. Duguet, *Meas. Sci. Technol.* **2**, 327 (1991).